

Measurement of neutron total cross-section of ^{93}Nb at J-PARC MLF ANNRI

S. Endo, A. Kimura, S. Nakamura, O. Iwamoto, N. Iwamoto, Y. Toh, M. Segawa,
M. Maeda and M. Tsuneyama
Japan Atomic Energy Agency, 2-4 Shirakata, Tokai-mura, Naka-gun, Ibaraki 319-1195
endo.shunsuke@jaea.go.jp

Abstract

The neutron total cross-section of Nb was measured by a transmission method to examine the resonance data by J-PARC MLF ANNRI. During the measurements, a diffraction effect of the Nb sample was remarkably observed. The diffraction effect of Nb was also studied since its effect cannot be ignored in deriving the neutron total cross-sections in a low energy region. As a result of the discussion by assuming a simple model including structure, it is clearly that the diffraction effect is not ignored below 0.2 eV. This article gives results of the neutron total cross-section measurement of Nb at J-PARC MLF ANNRI and discussions on the effect of diffraction.

1 Introduction

Niobium(Nb)-93, whose natural abundance is 100%, is one of material elements to strengthen stainless steel and is used in structural materials of nuclear reactors. Since Nb is also used as an element of superconductor alloys, it has been used in fusion reactors and accelerators. Niobium cause long-lived activities in stainless steel due to the long half-life of ^{94}Nb , about 20 thousand years [1]. Determination of resonance parameters with high accuracy are therefore required to estimate the activation. The cross-sections of Nb were measured by Wang *et al.* [2], Drindak *et al.* [4] and so on. The resonance parameters determined by them have discrepancies as shown in Table 1. In particularly, there are discrepancies larger than uncertainties between the results of Wang *et al.* and those of Drindak *et al.*. In order to determine which resonance parameters are more likely, measurements of neutron total cross-sections were performed at Accurate Neutron-Nucleus Reaction measurement Instrument (ANNRI) of Material and Life Science Experimental Facility (MLF) in Japan Proton Accelerator Research Complex (J-PARC).

Table 1: Resonance parameters for the first resonance of ^{93}Nb in past measurements

Reference	Resonance Energy [eV]	Γ_γ [meV]	$2g\Gamma_n$ [meV]
Wang+(2011)[2]	35.994 ± 0.0026	224.61 ± 20.82	0.0772 ± 0.0037
Meaze+(2011)[3]	35.92 ± 0.02	215.57 ± 17.98	0.078 ± 0.041
Drindak+(2006) [4]	35.992 ± 0.004	191 ± 8	0.125 ± 0.001
Sharapov+(1999) [5]	35.9	-	0.11 ± 0.01
Saplakoglu+(1958)[6]	35.9	205 ± 51	0.15 ± 0.01
Mughabghah 6th(2018)[7]	35.9 ± 0.1	218 ± 18	0.125 ± 0.010
JENDL-4.0(2010)[8] (=ENDF/B-VIII.0(2018)[9])	35.922	191	0.125

Table 2: The size of natural Nb target

Surface area	653.3 ± 5.7 [mm ²]
Thickness	10.2834 ± 0.0002 [mm]
Weight	56.1112 ± 0.0003 [g]
Surface density	$(5.567 \pm 0.049) \times 10^{-2}$ [/b]

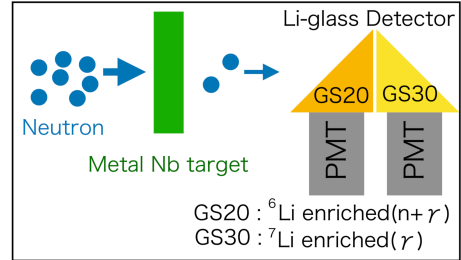


Figure 1: Experimental scheme

Table 3: Impurities contaminated in the Nb target

Element	Ta	Fe	O	C	N	others
Content [ppm]	2000	200	100	50	50	35

2 Experiment

Transmission measurements were performed at the ANNRI of MLF in J-PARC in June of 2019. In the MLF, neutrons were produced by spallation reactions of mercury targets [10]. The 3-GeV rapid cycling synchrotron, producing pulsed proton beam, was operated in double-bunch mode and 500-kW beam power with a repetition rate of 25 Hz at that time. The ANNRI is one of beamlines in the MLF, where Germanium gamma-ray detectors and Li-glass neutron detectors are installed to measure nuclear reactions. Cross-section measurements have been performed at the ANNRI [11].

Figure 1 shows the experimental scheme. Two types of Li-glass detectors were installed at ANNRI, one is ⁶Li-enriched (GS20) and the other one is ⁷Li-enriched (GS30). GS20 can detect γ -rays as well as neutrons in the reaction: ${}^6\text{Li} + n \rightarrow {}^3\text{H} + \alpha$. Time of flight (TOF) spectrum ascribed to only neutron can be obtained by subtracting the GS30 spectrum from the GS20 one. These Li-glass detectors were placed at 28-m flight length. Signals from detectors were processed by V1720 module made in CAEN, and pulse height and TOF were recorded in each event. Neutron total cross-section can be obtained by neutron transmission ratio. In order to determine the transmission ratio, measurements for beam open (blank) and Nb sample-in were performed for 10 hours and 12 hours, respectively.

The natural Nb target whose size was shown in Table 2 was used. Table 3 shows the impurities contaminated in Nb target. Since tantalum has similar chemical properties to Nb, it is included a little in Nb sample. In this article, when cross-section is derived, effects of Ta are not corrected because this effect is estimated to be the order of about 10^{-3} b in a region lower than 1 eV.

3 Analysis

3.1 Corrections

Figure 2 shows pulse-height spectra by GS20 and GS30 in the measurement of the Nb sample. GS30 has a slight sensitivity to neutron since ⁶Li is contained by about 0.01%. In order to remove noise and low-energy γ -rays backgrounds, threshold of pulse-height was set at 210 channel. Events were used when pulse-height is higher than the threshold. Dead-time corrections were made using a dead-time of 625 ns determined by the setting of the V1720 module.

In the present measurements, there are two types of backgrounds due to neutrons of flame-overlap and to γ -rays. First, the flame-overlap neutrons were estimated by following function:

$$f(t) = a \exp\left(-\frac{t-37}{t_1}\right), \quad (1)$$

where t represents TOF in ms and a and t_1 are fitting parameters. Flame-overlap effect was corrected by fitting this function to the TOF spectrum between 37 ms and 40 ms. Since the background events

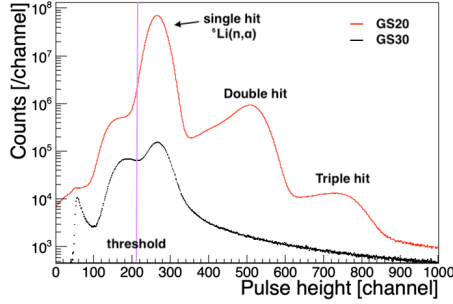


Figure 2: Pulse height spectra of GS20 (red line) and GS30 (black line) with threshold line (pink line)

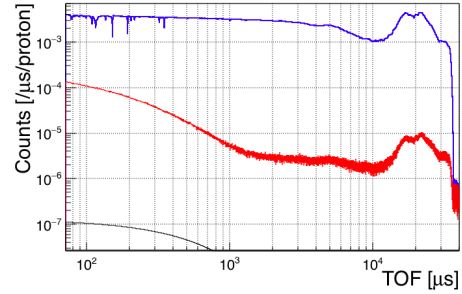


Figure 3: TOF spectra by Li-glass detectors A (blue line) and B (red line) and flame-overlap correction component (black line).

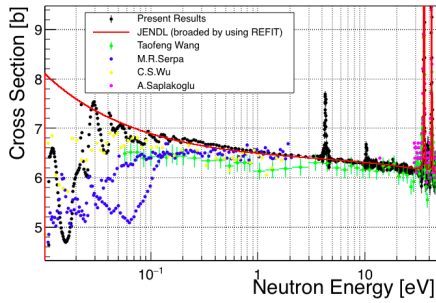


Figure 4: Neutron total cross-sections by the present and other past measurements at low energy

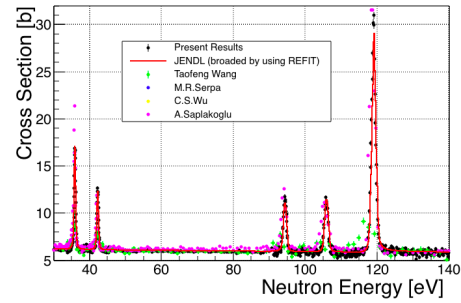


Figure 5: Neutron total cross-sections by the present and other past measurements at resonance region

by this effect were much smaller than true events, this correction has little effect on derivation of cross section.

Second, γ -rays backgrounds were removed by subtracting TOF spectrum of GS30 from that of GS20 as mentioned in Section 2. Figure 3 shows the TOF spectra of GS20 and GS30 and estimated flame-overlap correction component.

3.2 Derivation of total cross-sections

Transmission ratio (T) was obtained by dividing the Nb sample-in spectrum (Y_{sample}) by the blank spectrum (Y_{blank}). The cross-section can be derived from

$$\sigma(E) = -\frac{1}{n} \ln \frac{Y_{sample}}{Y_{blank}} = -\frac{1}{n} \ln T(E), \quad (2)$$

where n is the surface density. The obtained cross-sections are plotted in Fig. 4 and Fig. 5 in comparison with other past measurements and JENDL-4.0. The effects of resolution function and doppler broadening were considered in the figures of JENDL-4.0. The resonance at 4.3 eV is ascribed to ^{181}Ta . The cross-sections are fluctuated in a low energy region because of neutron diffraction. We thought this diffraction effects was observed clearly due to small capture cross-section of Nb (about 1.1 b at thermal energy). Wang *et al.* used spallation neutron sources as we did, while the other past group used nuclear reactor and fast chopper. Both of their results also are fluctuated in the same way as ours.

4 Estimation of neutron diffraction

4.1 The formalism of neutron diffraction

In the Nb measurements, neutron diffraction was clearly observed in a low energy region, and therefore we examined this neutron diffraction effect. Since the effect of neutron diffraction is due to crystal structure, it is not appropriate to discuss nuclear reactions in a single nucleus. For this reason, polycrystalline model (abbreviate this to “PCM” hereinafter) was used here for estimation of neutron diffraction.

In PCM, the total cross-section for scattering processes including neutron diffraction can be written [12] as:

$$\sigma_s(E) = \sigma_{\text{coh}}^{\text{b}} \left(S_{\text{coh}}^{\text{el}}(E) + S_{\text{coh}}^{\text{inel}}(E) \right) + \sigma_{\text{incoh}}^{\text{b}} \left(S_{\text{incoh}}^{\text{el}}(E) + S_{\text{incoh}}^{\text{inel}}(E) \right), \quad (3)$$

where each function $S(E)$ contains the information of sample system; $\sigma_{\text{coh}}^{\text{b}}$ and $\sigma_{\text{incoh}}^{\text{b}}$ are the bound coherent and incoherent cross-sections relating to cross-section σ :

$$\sigma^{\text{b}} = \left(\frac{A+1}{A} \right)^2 \sigma, \quad (4)$$

where $A = M/m$; M and m are target mass and neutron mass, respectively. For Nb, incoherent effects can be ignored since $\sigma_{\text{inc}}^{\text{el}}$ is negligibly small - about 0.038% against coherent effects. That is why the first term in Eq. (3) is only needed for estimation of neutron diffraction. The elastic coherent contribution of a polycrystalline solid can be given [12] by:

$$S_{\text{coh}}^{\text{el}}(E) = \frac{\pi^2 \hbar^2}{2mE v_0} \sum_{\tau_{hkl}}^{\tau_{hkl} < 2k_{\text{n}}} \frac{w(\tau_{hkl})}{\tau_{hkl}} \exp \left(-\frac{3\hbar^2 \phi_1(\Theta)}{2Mk_{\text{B}}\theta_{\text{D}}} \tau_{hkl}^2 \right), \quad (5)$$

where k_{n} , v_0 , \hbar , k_{B} and θ_{D} are neutron wave vector, the volume of the unit cell, the reduced Plank constant, Boltzmann constant and Debye temperature, respectively; $w(\tau_{hkl})$ is the multiplicity of reciprocal lattice vectors τ_{hkl} :

$$\tau_{hkl} = \frac{2\pi}{a} \sqrt{h^2 + k^2 + l^2}, \quad (6)$$

where a is lattice constant and h, k, l represent crystal planes. The ϕ_m term is described as:

$$\phi_m(\Theta) = \int_{-1}^1 d\varepsilon \varepsilon^m (e^{\varepsilon/\Theta} - 1)^{-1}, \quad (7)$$

where $\Theta = T/\theta_{\text{D}}$ and T is the absolute temperature. Here, inelastic coherent contribution involving phonons can be considered as the same as inelastic incoherent one [13]. The inelastic incoherent contribution [12-14] can be approximately expressed by the following equation:

$$S_{\text{inc}}^{\text{inel}}(E) = S_{\text{coh}}^{\text{inel}}(E) = \left(\frac{A}{A+1} \right)^2 \left\{ 1 + \frac{3}{4A} \phi_3(\Theta) \frac{k_{\text{B}}\theta_{\text{D}}}{E} \right\} - \frac{1}{12} \frac{Ak_{\text{B}}\theta_{\text{D}}}{E\phi_1(\Theta)} \left\{ 1 - \exp \left(-12 \frac{E}{Ak_{\text{B}}\theta_{\text{D}}} \phi_1(\Theta) \right) \right\}, \quad (8)$$

where the first term represents the total incoherent cross-section, consisted of elastic and inelastic incoherent processes, and the second term is the elastic incoherent one. Inelastic coherent cross-section can be obtained by Eq. (8) same as inelastic incoherent one.

Niobium crystal has a body-centered cubic lattice structure. In this case, summation in Eq. (5) is done when $h+k+l$ is even. Figure 6 shows cross sections calculated with PCM by Nb parameters listed in Table 4, and experimental results and calculated ones with free gas model (FGM). Cross sections by FGM are normalized to that by PCM at 8 eV.

Table 4: Niobium parameters used for PCM calculation

σ_{coh}	σ_{inc}	θ_{D}	a
6.253 [b] [7]	0.0024 [b] [7]	265 [K] [15]	3.3004 [Å] [16]

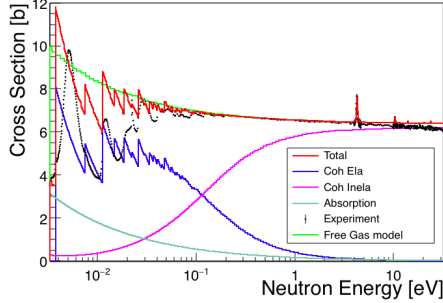


Figure 6: Cross-sections calculated with PCM and FGM and experimental results

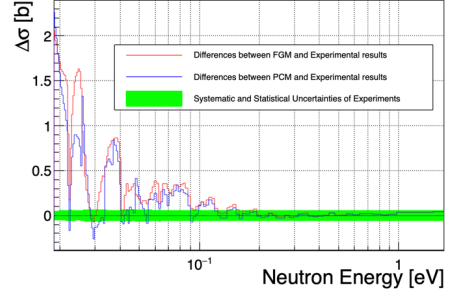


Figure 7: Differences between PCM, FGM and experimental results. Green band indicates statistical and systematic uncertainties of experimental results.

4.2 Discussion of neutron diffraction and evaluation of nuclear data

Figure 7 shows differences in FGM and PCM from experimental results. Green band indicates statistical and systematic uncertainties of experimental results. It is found that PCM has smaller discrepancy than FGM and that PCM can reproduce diffraction effects. Nevertheless, PCM is not enough to reproduce neutron diffraction effects. This might be due to the distortion of sample. From the region where the structure effect is not clear in PCM, it was decided not to use the present results below 0.2 eV below which the difference between PCM and experimental results is larger than experimental uncertainty. Uncertainty coming from the difference of the measured data might be also added to systematic uncertainty.

5 Summary

The transmission measurements at J-PARC MLF ANNRI were performed in order to obtain neutron total cross-sections of ^{93}Nb . In the Nb measurements, neutron diffraction was observed in the low energy region, and then this effect was examined with PCM. It became clearly that PCM can reproduce diffraction effects. However, since PCM is not enough to reproduce diffraction effects completely, It was decided not to use the present results below 0.2 eV. The total cross-sections obtained in this work will be analyzed with REFIT code to evaluate the resonance parameters.

Acknowledgments

The authors would like to thank staffs for their efforts in operating the accelerators and the neutron production target of J-PARC MLF. This work was supported in part by Grants-in-Aid for Scientific Research (JP17H01076).

References

- [1] M. Okoshi. Effects of Activation on the Dismantlement of Reactors - From the View Point of Radioactive Waste Management - RADIOISOTOPES. 1998 ;47:412-423
- [2] T. Wang *et al.* Measurements of neutron total cross-sections and resonance parameters of niobium using pulsed neutrons generated by an electron linac. 2011 ;289:945-952
- [3] A.K.M.M.H. Meaze and G.N. Kim. Determinations of niobium and palladium resonance cross-sections by time-of-flight transmission experiment. Indian J. Phys. 2011 ;85(2):329-338
- [4] N. J. Drindak *et al.* Neutron Capture and Transmission Measurements and Resonance Parameter Analysis of Niobium. Nuclear Science and Engineering. 2006 ;154:294-301
- [5] E. I. Sharapov *et al.* Search for parity violation in ^{93}Nb neutron resonances. Phys. Rev. C. 1999 ;59:1131-1135
- [6] A. Saplakoglu, L. M. Bollinger, R. E. Cote. Properties of s-Wave and p-Wave Neutron Resonances in Niobium. Phys Rev 1958 ;109:1258-1262
- [7] S. F. Mughabghab. Atlas of Neutron Resonances 6th ed, vol 1. Amsterdam: Elsevier; 2018
- [8] K. Shibata *et al.* JENDL-4.0: A New Library for Nuclear Science and Engineering. J. Nucl. Sci. Technol. 2011 ;48:1-30
- [9] B. A. Brown *et al.* ENDF/B-VIII.0: The 8th Major Release of the Nuclear Reaction Data Library with CIELO-project Cross Sections, New Standards and Thermal Scattering Data. Nuclear data sheets 2018 ;148:1-142
- [10] F. Maekawa *et al.* First neutron production utilizing J-PARC pulsed spallation neutron sources JSNS and neutronic performance demonstrated. Nucl Instruments Methods Phys Res Section. 2010; 620:159-165
- [11] K. Terada *et al.* Measurements of neutron total and capture cross sections of ^{241}Am with ANNRI at J-PARC. JNST. 2018 ;55:1198-1211
- [12] J. R. Gradana. Total scattering cross section of solids for cold and epithermal neutrons. Z. Naturforsch. 1984 ;39a:1160-1167
- [13] K. Binder. Total coherent cross section for the scattering of neutrons from crystals. Phys. Stat. sol. 1970 ;41:767-779
- [14] G. Placze and L. V. Hove. Interference effects in the total neutron scattering cross-section of crystals. Il Nuovo Cimento. 1955 ;1:233-256
- [15] C. Y. Ho, R. W. Powell, and P. E. Liley. Thermal Conductivity of the Elements: A Comprehensive Review. Journal of Physical and Chemical Reference data. 1974 ;3:1-796
- [16] M. E. Straumanis, and S. Zysczynski. Lattice parameters, thermal expansion coefficients and densities of Nb, and of solid solutions Nb-O and Nb-N-O and their defect structure. J. Appl. Crystallogr. 1970 ;3:1-6